Proton pump-rich cell secretes acid in skin of zebrafish larvae

Li-Yih Lin,[1,2] Jiun-Lin Horng,[1,3] Joseph G. Kunkel,[4] and Pung-Pung Hwang[1,3]

[1]*Institute of Cellular and Organismic Biology, Academia Sinica, Taipei,* [2]*Department of Physical Therapy, Shu-Zen College of Medicine and Management, Kaohsiung, and* [3]*Graduate Institute of Life Sciences, National Defense Medical Center, Taipei, Taiwan, Republic of China; and* [4]*Department of Biology, University of Massachusetts, Amherst, Massachusetts*

Lin, Li-Yih, Jiun-Lin Horng, Joseph G. Kunkel, and Pung-Pung Hwang. Proton pump-rich cell secretes acid in skin of zebrafish larvae. *Am J Physiol Cell Physiol* 290: C371–C378, 2006. First published September 7, 2005; doi:10.1152/ajpcell.00281.2005.—The mammalian kidney excretes its metabolic acid load through the proton-transporting cells, intercalated cells, in the distal nephron and collecting duct. Fish excrete acid through external organs, gill, or skin; however, the cellular function is still controversial. In this study, molecular and electrophysiological approaches were used to identify a novel cell type secreting acid in skin of zebrafish (*Danio rerio*) larvae. Among keratinocytes covering the larval surface, novel proton-secreting ionocytes, proton pump (H^+-ATPase)-rich cells, were identified to generate strong outward H^+ flux. The present work demonstrates for the first time, with a noninvasive technique, H^+-secreting cells in an intact animal model, the zebrafish, showing it to be a suitable model in which to study the functions of vertebrate transporting epithelia in vivo.

hydrogen-adenosinetriphosphatase; ionocytes; epithelial transport; ion-selective electrode

THE ZEBRAFISH (*Danio rerio*) occupies a prominent position in developmental biology. It is increasingly being recognized as a useful model for studying vertebrate organogenesis as well as the function of whole organs or an entire organism (1, 3). During fish embryonic stages, the skin is believed to regulate body fluid pH and ionic composition before the development and functioning of gills, kidneys, and intestine (15, 17, 20, 24, 25). Skin of zebrafish embryos or larvae may be an excellent model to study the functions of vertebrate transport epithelia and their ionocytes, because the embryonic skin is comparatively easy to use for morphological observations and functional assays in vivo.

In mammals, the kidney excretes the metabolic acid load through the proton-transporting cells, the intercalated cells, in the distal nephron and collecting duct (2, 4). Intercalated cells are often referred to as "mitochondria-rich" (MR) cells because they contain large numbers of mitochondria. Fish excrete acid mainly through their gills, where MR cells are also found (10). In freshwater fish, the apical V-type H^+-ATPase has been proposed to pump out H^+ and simultaneously generate an electrical gradient for Na^+ uptake from water in gill epithelial cells (10). However, our knowledge of the exact site and mechanisms of H^+ secretion is still controversial and incomplete. Two major cell types, pavement cells and MR cells composing the epithelium of gills, are thought to conduct these ion transport functions. H^+-ATPase was immunolabeled on the apical regions of pavement cells and MR cells in freshwater

trout (*Oncorhynchus mykiss*) (26). However, in freshwater tilapia (*Oreochromis mossambicus*), H^+-ATPase exclusively localized to pavement cells (35). Recently, Katoh and associates (21) cloned the H^+-ATPase A subunit from freshwater-adapted killifish (*Fundulus heteroclitus*) and localized the protein in the basolateral membrane of branchial MR cells. Although the inconsistent evidence may reflect variation among fish species, convincing electrophysiological and molecular evidence is still lacking to demonstrate which cell type transports protons. In the present work, we used an electrophysiological technique, the scanning ion-selective electrode technique (SIET), to find a novel cell type secreting protons in skin of intact zebrafish larvae and, using immunocytochemistry and in situ hybridization, demonstrated that these cells express abundant H^+-ATPase.

MATERIALS AND METHODS

Zebrafish. Mature zebrafish (AB strain) were reared in circulating tap water at 28°C. Fertilized eggs were incubated in "zebrafish solution," which contained (in mM) 0.4 NaCl, 0.2 $MgSO_4$, 0.08 K_2HPO_4, 0.005 KH_2PO_4, and 0.2 $CaSO_4$ (pH 6.8). The ionic composition of the zebrafish solution reflects the local tap water composition. Hatched zebrafish larvae at 72 h after fertilization were used for the subsequent experiments. The experimental protocols were approved by the Academia Sinica Institutional Animal Care and Utilization Committee (approval no. RFiZOOHP2002086).

RNA probe synthesis. A fragment of the V1 subunit A of zebrafish H^+-ATPase (BC055130), nucleotides 407–1143, was obtained using PCR and inserted into the pGEM-T easy vector (Promega, Madison, WI). Purified plasmids were then linearized using restriction enzyme digestion, and in vitro transcription was performed with T7 and SP6 RNA polymerase (Roche, Penzberg, Germany). Digoxigenin (Dig)-labeled RNA probes were examined using RNA gels and dot blot assay to confirm quality and concentration.

Whole mount in situ hybridizations. After an initial overnight fixation with 4% paraformaldehyde in 0.1 M phosphate buffer (PB; pH 7.4) at 4°C, embryos were kept in 100% methanol. The embryos were incubated for 10 min each in 50% MeOH in PB + 0.09% NaCl (PBS) with 0.1% Tween 20 (PBST) and 30% MeOH in PBST and twice in PBST and then were treated with proteinase K (10 μg/ml) for 20 min. After a brief rinse with PBST, the embryos were fixed with 4% paraformaldehyde for another 20 min. After PBST washing, the samples were incubated with hybridization buffer (HyB, 50% formamide, 5× SSC, 0.1% Tween 20) at 65°C for 5 min and with HyB with 500 μg/ml yeast tRNA at 65°C for 2 h before hybridization. After an overnight hybridization with 100 ng/ml Dig-labeled antisense or sense RNA probes, the embryos were washed serially with 50% formamide-2× SSC (65°C, 20 min), 2× SSC (65°C, 10 min), 2× SSC-0.1% Tween 20 (SSCT; 65°C, 10 min), 0.2× SSCT (65°C, 10 min, 2 times), and PBST [room temperature (RT), 10 min]. Thereafter, the embryos were immnunoreacted with an alkaline phosphatase-

coupled anti-Dig antibody (1:5,000) and then were treated with nitro blue tetrazolium and 5-bromo-4-chloro-3-indolyl phosphate for the alkaline phosphatase reaction. Samples were observed with a stereomicroscope (SZX-ILLD100, Olympus, Tokyo, Japan) or an upright microscope (BX-50WI, Olympus), depending on the image size desired.

Whole mount immunocytochemistry. To double stain for Na$^+$ pump (Na$^+$-K$^+$ ATPase) and H$^+$ pump (H$^+$-ATPase), zebrafish larvae were anesthetized on ice and fixed with 4% paraformaldehyde in 0.1 M PB (pH 7.4) for 1 h at 4°C. After being rinsed with PBS, the larvae were postfixed and permeabilized with 70% ethanol at -20°C for 10 min. After being washed with PBS, samples were incubated with 3% bovine serum albumin and 5% normal goat serum for 30 min to block nonspecific binding. The larvae were then incubated overnight at 4°C with α5 monoclonal antibody against the α-subunit of the avian Na$^+$ pump (diluted 1:200 with PBS; Developmental Studies Hybridoma Bank, University of Iowa), and polyclonal antibody against the A subunit of killifish H$^+$-ATPase (21). After being rinsed with PBS for 20 min, the larvae were further incubated in goat anti-rabbit IgG conjugated with FITC and goat anti-mouse IgG conjugated with Texas red (diluted 1:100; Jackson Immunoresearch Laboratories, West Grove, PA), for 2 h at RT (26–28°C).

For triple staining of concanavalin A (ConA), Na$^+$ pump, and H$^+$ pump, live larvae were preincubated in zebrafish solution containing 0.5 mg/ml Texas red-conjugated ConA (Molecular Probes, Eugene, OR) for 10 min. After being washed in normal zebrafish solution for 3 min, the ConA-labeled larvae were fixed and immunostained as described above, except that secondary antibodies were used. Goat anti-rabbit IgG conjugated with Cy5 and goat anti-mouse IgG conjugated with FITC (diluted 1:100; Jackson Immunoresearch Laboratories) were used as secondary antibodies.

For double staining of Na$^+$ pump and mitochondria, MitoTracker Deep Red (M-22426, Molecular Probes) and MitoTracker Green FM (M-7514, Molecular Probes) stock solutions were prepared in DMSO. Larvae were vital stained with MitoTracker Deep Red in a final concentration of 1 μM in water for 10 min. After fixation, samples were permeabilized and blocked following the stain process described previously for Na$^+$ pump. For double staining of ConA and mitochondria, larvae were first stained with 0.5 mg/ml Texas red-conjugated ConA for 10 min and then with MitoTracker Green FM (1 μM in water) for another 10 min.

Observations and image acquisitions were made with a Leica TCS-NT confocal laser scanning microscope (Leica Lasertechnik, Heidelberg, Germany) equipped with $\times 10$$-$0.3 numerical aperture (NA), $\times 20$$-$0.4 NA, $\times 40$$-$1.2 NA, and $\times 100$$-$1.35 NA lenses and appropriate filter sets for simultaneous monitoring of various fluorescences.

Scanning ion-selective electrode technique. SIET (12, 22) was used to measure extracellular H$^+$ flux and H$^+$ activity (pH) at the surface of zebrafish larvae. Microelectrodes with tip diameters of 3–4 μm were pulled from glass capillary tubes (World Precision Instruments, Sarasota, FL; no. TW 150-4 with 1.12- and 1.5-mm inner and outer diameters, respectively) with a Sutter P-97 Flaming Brown pipette puller (Sutter Instruments, San Rafael, CA). These were then baked in covered dishes at 200°C overnight and vapor silanized with dimethyl chlorosilane (Fluka, Buchs, Switzerland) for 30 min, and the covers were removed before further baking at 200°C for at least 1 h. H$^+$-selective microelectrodes were made as previously described (12). The capillaries were backfilled with a 1-cm column of 100 mM KCl-H$_2$PO$_4$ (pH 7.0) and then frontloaded with a 20- to 30-μm column of liquid ion exchanger cocktail (Hydrogen Ionophore I-cocktail B; Fluka). The ion-selective microelectrode was connected to an operational amplifier (IP Amp ion polarographic amplifier; Applicable Electronics, East Falmouth, MA) via an Ag/AgCl wire electrode holder (World Precision Instruments), and the circuit was completed by placing a salt bridge (3 M potassium acetate, 10 mM KCl in 3% agarose connected to a Ag/AgCl wire).

Electrode vibration and positioning were achieved with a stepper motor-driven three-dimensional (3D) positioner (Applicable Electronics). Data acquisition, preliminary processing, and control of the 3D electrode positioner were performed with ASET software (Science Wares, East Falmouth, MA). A direct voltage-measuring electrode was oscillated with an excursion distance of 10 μm. The typical cycle was completed in 3–4 s. A cycle includes an adjustable settling time after each move, one direct voltage measurement period at each extreme of the cycle, and the excursion time. The measurement taken nearest to the tissue is subtracted from the measurement taken at the opposite end of the cycle. This subtraction provides the self-referencing feature of the probe.

The vibrating electrode system was attached to an Olympus upright microscope (BX-50WI). A $\times 10$ dry and a $\times 40$ water immersion objective lens (working distance 3.3 mm) were used for differential interference contrast (DIC) imaging. The microscope equipped with a charge-coupled device camera allowed images to be visualized on a color monitor and recorded with a frame grabber controlled by the ASET software.

Calibration of ion-selective vibrating probe. Before the collection of biological data, the efficiency of the H$^+$ probe was determined using a method published previously (12). Efficiency of the H$^+$ probe depends on several factors, including the properties of the ionophore, data acquisition, and particularly buffer concentration. In our directly coupled system, the efficiency of the H$^+$ probe is close to 100%. The Nernstian properties of each electrode were measured by placing the electrode in a series of standard pH solutions (pH 6, 7, and 8). When the voltage output of the probe was plotted against log H$^+$ activity, linear regression yielded a Nernstian slope of 57.8 (SD 2.3) ($n = 10$).

Surface pH of zebrafish larvae. SIET was performed at RT (24–26°C) in a small plastic recording chamber filled with 1 ml of "recording solution" that contained zebrafish solution, 300 μM MOPS buffer (Sigma, St. Louis, MO), and 0.1 mg/l ethyl 3-aminobenzoate (Tricaine, Sigma; pH = 6.8). An anesthetized larva [1 day posthatching (dph)] was positioned in the center of the chamber with its lateral side contacting the base of the chamber. To record the surface pH surrounding the larvae, the probe was moved to the six selected positions, which were ~20 μm away from the larval surface at snout, pericardial cavity, ventral yolk sac, lateral yolk sac, trunk, and tail (as shown in Fig. 1A). Voltage output signals in millivolts were recorded every 3.0 s and averaged for 3.0 min at every position. The averaged voltages were converted to H$^+$ activity and pH value after three-point calibration (pH 6, 7, and 8). After recording of the six positions, the larva was removed from the chamber to record the background values of the medium.

H$^+$ flux in keratinocytes and ionocytes. An anesthetized larva was laid laterally in the chamber for the following measurement. Under the DIC microscope, the apical membrane of ionocytes could be easily identified in the skin covering the entire larva, except in yolk sac regions, where the numerous granules in the yolk interfered with identification. Therefore, most ionocytes measured in this study were distributed on the skin covering the lateral side of the body trunk, which also served as a suitable flat plane for probing. To detect local H$^+$ flux generated by specific cells, the probe was moved to ~2–3 μm above the surface spot of interest. A "line scan" was made by probing a series of spots composing a line (40 μm with 9 spots) across the surface of the ionocytes and adjacent keratinocytes (as shown in Fig. 5A). At every spot, voltage difference in microvolts (which was further converted to H$^+$ flux) was measured by SIET orthogonal to the measured surface.

The specific H$^+$ pump inhibitor bafilomycin A1 (Sigma B-1793) was also used to examine the inhibitory effects on proton secretion at the apical surface of ionocytes. Bafilomycin A1 was dissolved in DMSO and added to the recording chamber at final concentrations of 1 and 10 μM. SIET probing was performed at the surface of putative "H$^+$ pump-rich cells" (HR cells) that were identified on the yolk tube epithelium of larvae (see below). For these probes, voltage differences
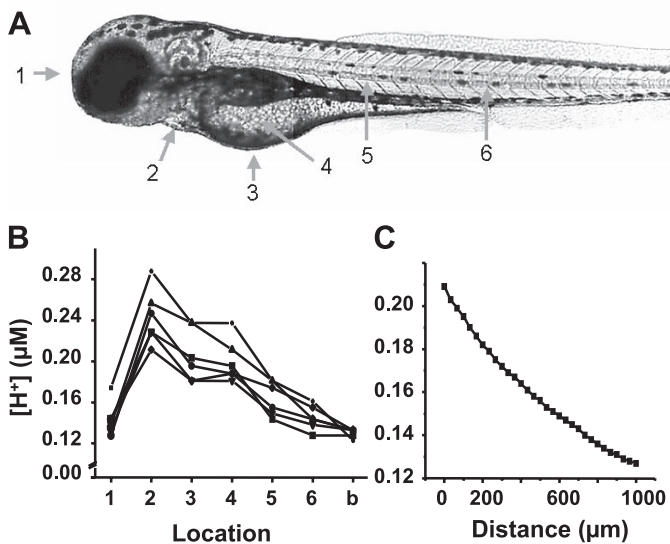
Fig. 1. Surface pH gradients in zebrafish larvae. *A*: 6 locations at snout (*1*), pericardial cavity (*2*), ventral yolk sac (*3*), lateral yolk sac (*4*), trunk (*5*), and tail (*6*) of the larvae. *B*: calculated H^+ activities ($[H^+]$); each line connects the 6 probed locations on 6 individual larvae and the background (b). The 6 larvae showed consistently high H^+ activity at pericardial and yolk sac surfaces. When the probe was moved away from the yolk sac, H^+ activity declined with distance to the larva (*C*).

>1,000 μV were recorded and considered as H^+ secretion from HR cells. Effects of bafilomycin A1 on H^+ secretion were recorded in 15 HR cells from 15 individuals (5 individuals for each treatment).

RESULTS

Surface pH of zebrafish larvae. Surface pH of 1-dph larvae was measured using SIET to determine the pH gradients generated by the larvae (Fig. 1). Six locations on different surfaces of the larvae and background (removal of the larvae) were chosen for measurement (Fig. 1*A*). When a larva was placed in the chamber for measurement, the H^+ activity surrounding the larva gradually increased and reached a plateau within 10 min, indicating net H^+ flux outward from the larva and gradually generating a constant pH gradient. Figure 1*B* shows the H^+ activity measured at the six selected locations from six 1-dph larvae and backgrounds. The highest H^+ activity was detected at the surface of the pericardial cavity [*location 2*, 0.243 μM (SD 0.027); $n = 6$], which was about twice background [0.13 μM (SD 0.004); $n = 6$]. When the probe was moved from the pericardial surface toward the two ends of the larva, the H^+ gradient gradually declined. At snout and tail surface (*locations 1* and *6*, respectively), H^+ activity dropped to close to background level. The highest H^+ gradient at the pericardial or yolk sac surface suggests that a larger integrative excretion of H^+ occurs at these locations. As the probe was moved away from the surface of the larva, a gradual decline of H^+ activity was measured (Fig. 1*C*). These surface-probing data indicate that the large surface of the yolk sac is a major source of H^+ flux.

Localization of H^+ pump and Na^+ pump. To identify the specific cell type responsible for the H^+ excretion, in situ hybridization with H^+ pump mRNA and double immunolabeling of H^+ pump and Na^+ pump in zebrafish larvae were conducted. The antibody used for this work was shown to react with the antigens from zebrafish in preliminary work (Western blot analysis; data not shown). H^+-ATPase mRNA was expressed in the specific cells on the skin covering the yolk sac and its extension, the yolk tube (Fig. 2, *A* and *B*), but very few signals were observed in the skin of the trunk (Fig. 2, *A* and *B*). No significant H^+-ATPase mRNA was found in polygonal keratinocytes, which cover most surfaces of the larva (Fig. 2, *A* and *B*). The H^+ pump protein was found unevenly over the entire larval skin. Immunostaining signals of H^+ pump were
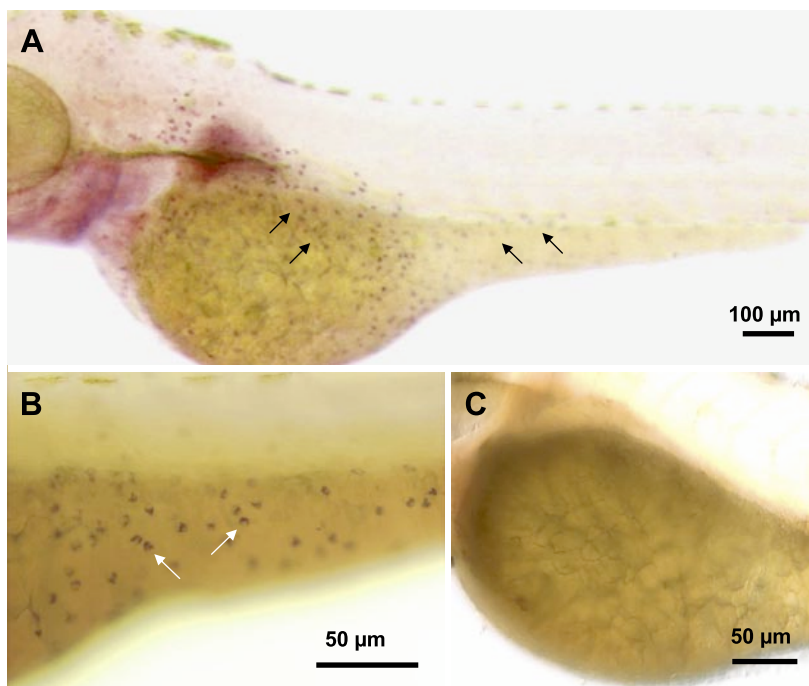
Fig. 2. In situ hybridization of H^+-ATPase subunit A in 72-h posthatching larvae. H^+-ATPase mRNA was expressed in the cells located in the skin of yolk sac and yolk tube area (arrows in *A* and *B*); however, the signal was seldom found in the skin of the trunk (*A* and *B*). No signal was found in larval skin with the sense probe (*C*).

weak in polygonal keratinocytes and considered as background signals (green signal in Fig. 3, *A* and *B*). Particularly strong and concentrated signals were found in a group of smaller cells dispersed on the yolk sac and yolk tube (Fig. 3, *A–D*), corresponding to the distribution of the H$^+$-ATPase mRNA-expressing cells as described above (Fig. 2, *A* and *B*). These oval HR cells expressed the H$^+$ pump highly in the apical membrane domain and less in the cytoplasm (*xy*-plane of image shown in Fig. 3*C*; *z*-plane of image shown in Fig. 3*D*). Simultaneously, Na$^+$ pump localization was also examined to identify the ionocytes, or MR cells. Interestingly, the Na$^+$ pump was not detectable in the HR cells but in another group of cells distributed on yolk sac, yolk tube, and even the trunk area of larvae (Fig. 3, *A–D*). These Na$^+$ pump-rich cells (NaR cells) were identified as typical MR cells (3), which featured high Na$^+$ pump expression in tubule-like enfolding of baso-lateral membrane (Fig. 3*D*) and numerous mitochondria labeled with the fluorescent probe MitoTracker (Fig. 4, *A* and *B*).

Labeling of ConA on apical membrane of HR cells. For the subsequent probing of H$^+$ flux in a single cell, a convincing in vivo method was needed to distinguish HR cells from other cells. The lectin ConA has been found to be a marker for the apical membranes of gill ionocytes (34). Figure 3, *E* and *F*, shows the confocal image of the triple labeling of Texas red-conjugated ConA, H$^+$ pump, and Na$^+$ pump (red, blue, and green signals, respectively) in a whole larva. ConA is shown to bind the apical membrane of HR cells but not that of NaR cells (Fig. 3*E*). Figure 3*F* shows the extracted signal of ConA from the triple labeling. Ninety-eight percent of HR cells analyzed ($n = 101$) were ConA positively stained; however, none of the NaR cells ($n = 104$) was positively labeled. On basis of these results, ConA is a faithful marker to discriminate
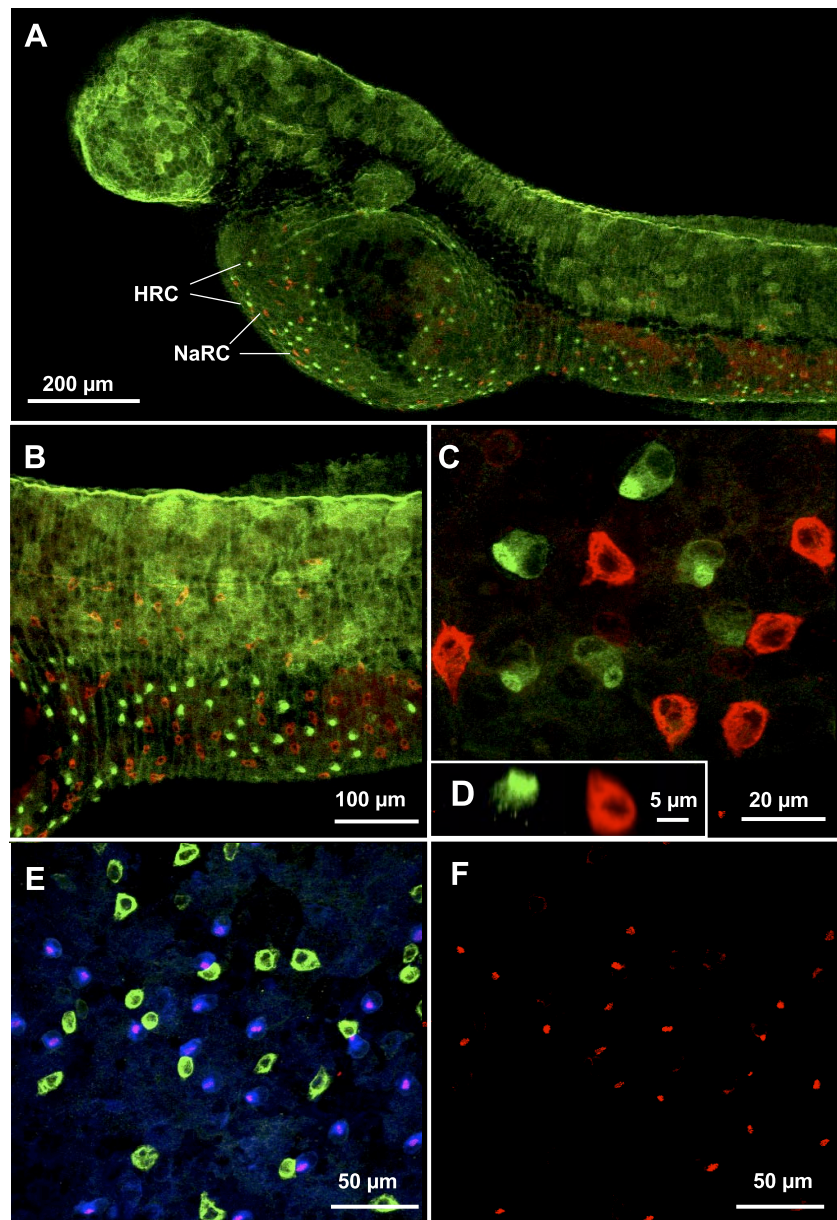
Fig. 3. Confocal images of larval skin with immunocytochemical labeling. *A–C*: double staining for H$^+$ pump (green signals) and Na$^+$ pump (red signals). Polygonal keratinocytes covering most surfaces of larvae express H$^+$ pump (with variable staining intensity; *A* and *B*). The oval H$^+$ pump-rich cells (HRC), which express H$^+$ pump highly in apical membrane and less in cytoplasm (*xy*-plane image, *C*; *z*-plane image, *D*), dispersed on the yolk sac and yolk tube (*A* and *B*). The Na$^+$ pump was not detectable in HRC but was in another cell type, Na$^+$ pump-rich cells (NaRC), which are distributed on the yolk sac, yolk tube, and trunk surface of larvae (*A–C*). *E*: triple staining of H$^+$ pump, Na$^+$ pump, and concanavalin A (ConA). *F*: extracted signal of ConA from the triple labeling. ConA-Texas red (pink signals in *E*, red signals in *F*) was found to bind the apical membrane of HRC (blue signals) instead of NaRC (green signals) (*E* and *F*).
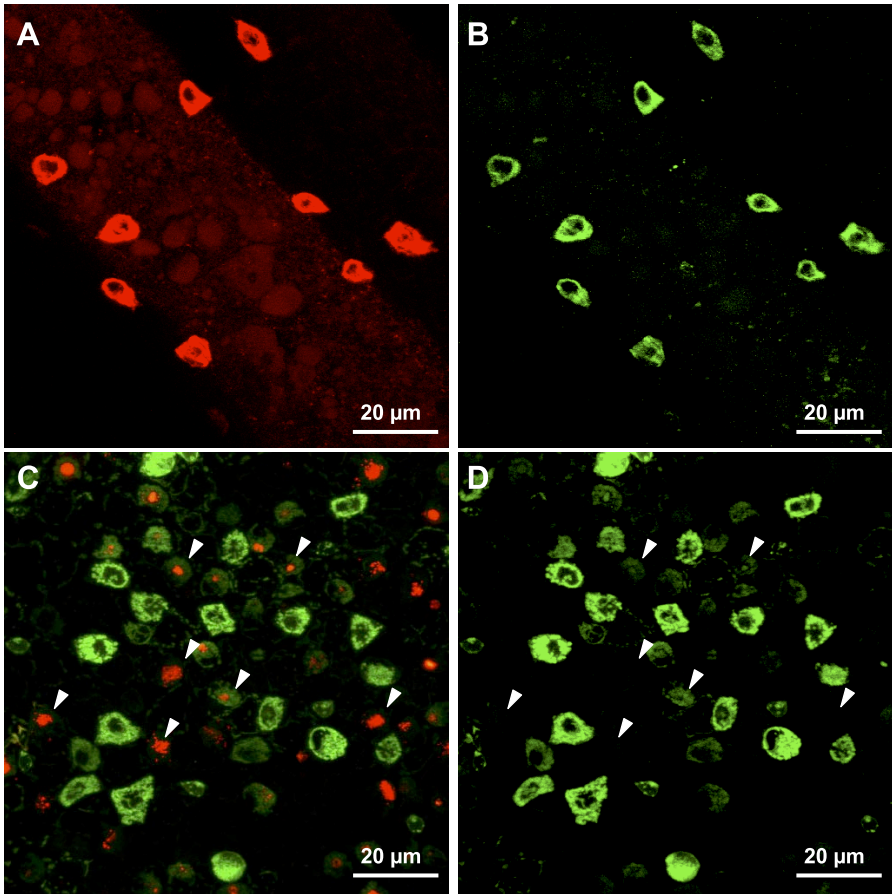
Fig. 4. Confocal images of larval skin with immunocytochemical labeling. Double staining of Na$^+$ pump (red signals, *A*) and mitochondria (stained with MitoTracker; green signals, *B*) is shown. Red signals and green signals are completely merged in the same cell, indicating that the NaRC are the mitochondria-rich cells. *C* and *D*: double staining of ConA-Texas red (red signals) and mitochondria (green signals) and green signals alone. The ConA-Texas red signals indicate the locations of HRC shown in Fig. 3*D*. These ConA-Texas red-labeled HRC (arrowheads) are relatively faint in green signals, indicating that the HRC are mitochondria poor (*C* and *D*).

these two groups of cells. With double staining of ConA-Texas Red and the mitochondria fluorescent probe MitoTracker, HR cells were investigated to determine whether they featured numerous mitochondria as NaR cells did. Confocal images showed that ConA-labeled HR cells were substantially weaker in MitoTracker signal than NaR cells, indicating that HR cells are poor in mitochondria quantity (Fig. 4, *C* and *D*).

H$^+$ flux in keratinocytes and ionocytes. The H$^+$ flux probe was not directly conducted on these ConA-labeled larvae, because physiological properties of the cells might be altered by ConA binding. Instead, ConA labeling was used to discriminate cells after these cells had been probed. Under the DIC microscope, polygonal keratinocytes and oval cells with apical membranes surrounded by keratinocytes could be identified on larval surfaces (Fig. 5*A*). After the H$^+$ flux probe across the oval cell apical membranes, the live larvae were labeled with ConA. Positively stained HR cells were found in a portion of these oval cells (Fig. 5, *B* and *C*). In contrast, the other ConA negatively stained cells may contained NaR cells and/or other unidentified cells. The line scan of SIET was done across the apical membrane of the cells from six individuals. Figure 6*A* shows an image automatically grabbed by the system after a line scan (40 μm with 8 intervals) over a target cell. Voltage differences and calculated H$^+$ fluxes of line scans over 12 target cells from one of the six probed larvae are shown in Fig. 6*B* after these probed cells were discriminated into ConA-positive (ConA$^+$) and -negative (ConA$^-$) groups. The probe detected weaker outward flux of H$^+$ on keratinocytes but

gradually increased when probing toward the apical membrane of the ConA$^+$ cells (Fig. 6*B*). The surge of H$^+$ efflux appearing right on the apical side of ConA-labeled cells strongly suggests that these HR cells play a critical role of pumping H$^+$ out of the larvae. In contrast, no surge of signal was found when probing the surface of ConA$^-$ cells (Fig. 6*B*). For statistical comparison, the H$^+$ effluxes on apical sites of both ConA$^+$ and ConA$^-$ cells (usually the central points of the line scans) and keratinocytes (the two end points of the line scans on ConA$^-$ cells) were analyzed (Fig. 6*C*). The negligible background values represent the noise signals recorded by line scan in medium without animals (Fig. 6*C*). The H$^+$ fluxes of ConA$^+$ cells are significantly higher than those of ConA$^-$ cells or keratinocytes, even though they are quite variable. There is no significant difference between ConA$^-$ cells and keratinocytes, indicating that H$^+$ flux from ConA$^-$ cells is subtle or lacking.

With the specific inhibitor of V-type ATPase bafilomycin A1, H$^+$ secretion from ConA$^+$ cells (HR cells) was examined. Figure 7*A* shows that the voltage difference of H$^+$ (outward H$^+$ flow) at the surface of HR cells declines gradually after 10 μM bafilomycin A1 is applied. After 10-min treatment with bafilomycin A1, H$^+$ flux declined to a stable and minimal level (further applied inhibitor did not decrease the flux significantly). As shown in Fig. 7*B*, the inhibitory effects of bafilomycin A1 on H$^+$ flux indicate a dose-dependent pattern. In contrast, bafilomycin A1 does not alter the subtle H$^+$ flux from the keratinocytes (data not shown), indicating that the out-
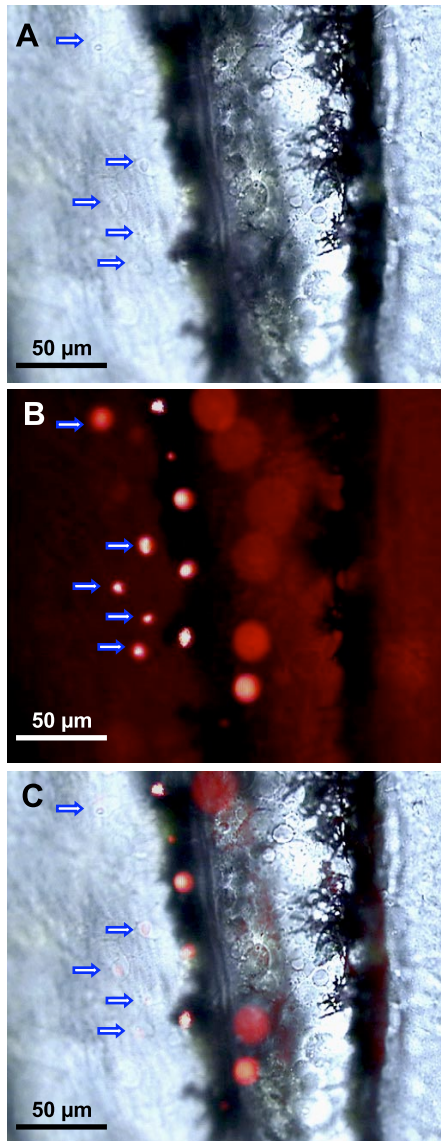
Fig. 5. Discrimination of ConA-positive (ConA⁺) and ConA-negative (ConA⁻) cells. After scanning ion-selective electrode technique (SIET) probing, the larvae were stained with ConA-Texas red and observed with the differential interference contrast (DIC) microscope-equipped fluorescence apparatus. Images were grabbed under DIC microscopy with (*A*) or without (*B*) fluorescent excitation, and images of the two were merged (*C*). ConA fluorescence (red signal) is clearly localized on the apical membrane of partial oval cells, which correspond to the HRC (arrows). Diffused and greater ConA fluorescence reveals out-of-focus signals.

domain and generated strong outward H⁺ flux, which could be blocked by a specific inhibitor of H⁺ pumps. In the present study, for the first time, a noninvasive technique was used to detect H⁺ flux from a single cell in an intact animal, which suggests that the skin of the zebrafish embryo or larva is a suitable model in which to study the functions of vertebrate transporting epithelia in vivo.

SIET was developed to enable a noninvasive measurement of ion flux from isolated tissue and cells (22). Several reviews have addressed the application of this technique in various systems (5, 32, 33). Jaffe and Nucitelli (19) first developed and applied the "vibrating probe" or "vibrating voltage probe" technique to biological systems, and the technique was later modified into the "ion-selective vibrating probe" (SIET) or, in short, the "vibrating ion probe" (18). The early vibrating probe technique was used in studying transepithelial ion flux in fish
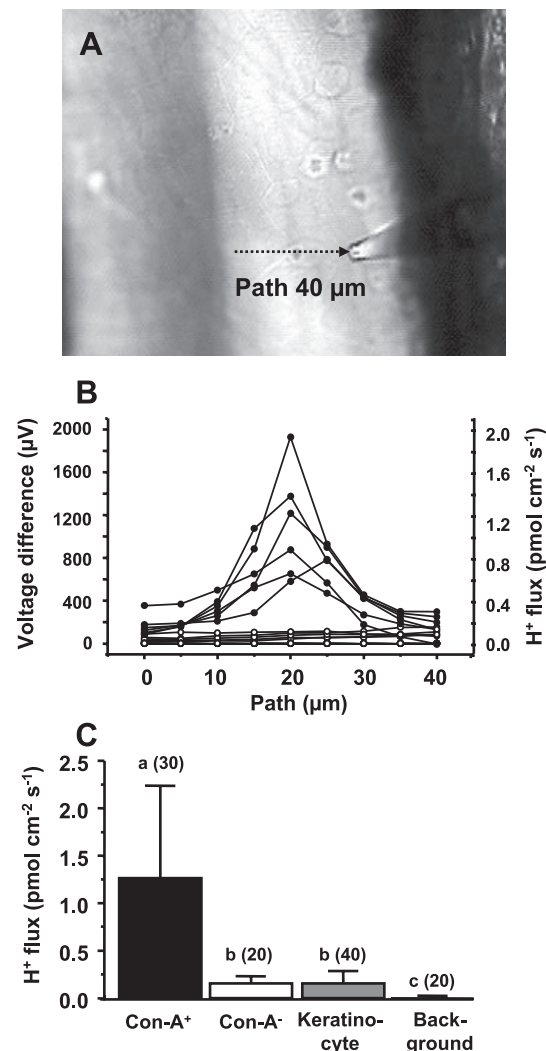
Fig. 6. H⁺ flux in keratinocytes and ionocytes. Under DIC microscopy, apical membranes of ionocytes were identified, and a "line scan" was made by probing at series of locations composing a line (arrow) across the surface of the ionocytes and adjacent keratinocytes (*A*). *B*: voltage differences and calculated H⁺ fluxes of a line scan over 12 target cells from 1 of the 6 probed larvae after these probed cells were discriminated into the ConA⁺ (●) or Con-A⁻ (○) group. *C*: H⁺ effluxes (means + SD) from different types of cells were compared. Different letters indicate significant difference (1-way ANOVA, $P < 0.05$).

flow of proton from keratinocytes may not be associated with V-type ATPase.

DISCUSSION

With a noninvasive electrophysiological technique (SIET), this study has demonstrated proton secretion in the skin of live zebrafish larvae. A H⁺ gradient generated by H⁺ secretion was detected surrounding the entire larval surface, with the strongest signal found at the yolk sac and pericardial surface. Most important, this study has identified a novel proton-secreting ionocyte, H⁺ pump-rich (HR) cell, in larval skin. HR cells expressed numerous H⁺ pumps in their apical membrane

A

B

Fig. 7. Effects of bafilomycin A1 on proton secretion at the apical surface of HR cells. *A*: signals of voltage difference recorded with SIET. Positive values indicate outflow of H^+ current. Asterisk indicates background signal recorded at 100 μm from the surface of larvae. Arrows indicate the application of 10 μM bafilomycin A_1 or DMSO (control). The time scale is continuous, but larger artifacts from drug application have been erased from the traces. After 10-min treatments, the declined % of voltage differences were counted and compared (*B*). Different letters indicate significant difference (1-way ANOVA, $P < 0.05$).

and frog models. Foskett and Scheffey (13) first used the vibrating probe to detect Cl^- excretion from chloride cells (the original term for MR cells) in isolated opercular epithelium of seawater-adapted fish, and the work is a landmark study in fish MR cells.

During the past two decades, the salt-secreting function of the branchial ionocytes, MR cells, in seawater fishes has been extensively studied; however, MR cells seem to display more complicated functions in freshwater fishes than in seawater fishes. The branchial epithelium of fish is thought to be responsible for taking up several ions, including Na^+, Cl^-, and Ca^{2+}, from very diluted freshwater. There is a tight linkage between NaCl uptake and acid-base regulation, because Cl^- is removed from the freshwater in exchange for a basic equivalent (HCO_3^-), whereas Na^+ is removed from the water in exchange for an acidic equivalent (H^+). V-type H^+-ATPase has been demonstrated to drive Na^+ uptake through a coupled Na^+ conductive channel and/or to associate with Cl^- uptake via a Cl^-/HCO_3^- exchanger in frog skin (11, 23). A similar mechanism has been proposed in gills of freshwater fishes (7, 27, 29); however, the exact sites for H^+ secretion are still a controversial subject (see introduction). Two major cell types, pavement cells and MR cells composing the surface of gills, are thought to conduct these ion transport functions. In this study, we found that both keratinocytes and a group of ionocytes (HR cells) in the skin of zebrafish larvae are involved in H^+ secretion. The H^+ flux in keratinocytes was lower than that in HR cells.

However, only HR cells showed V-type ATPase-dependent proton flux. The subtle proton outflow in keratinocytes might occur through an unidentified transporter or might simply be diffusion of CO_2 gas.

Another important finding in this study is the identification of two groups of ionocytes (HR cells and NaR cells) differentially distributed on larval skin. NaR cells, featuring Na^+ pump-rich, infolded basolateral membrane and numerous mitochondria, were identified as typical MR cells; however, HR cells lacked these features. A functional difference was clearly found between these two groups of cells; only HR cells produced a large outward H^+ current. The existence of MR cell subtypes in freshwater fish has been proposed in several reports; however, it is still a debatable and challenging subject (8, 9, 14, 30). Recently, Goss and colleagues (14, 31) isolated peanut lectin agglutinin (PNA)-labeled (PNA$^+$) and nonlabeled (PNA$^-$) MR cells from rainbow trout gills; both cell types expressed H^+-ATPase and Na^+-K^+-ATPase, and in in vivo experiments only the PNA$^-$ MR cells demonstrated phenamil- and bafilomycin-sensitive acid-activated Na^+ uptake. In vivo immunochemical and physiological evidence is necessary to confirm whether the PNA$^-$ MR cells are homologs of the HR cells in the present study. Recent studies in tilapia acclimated to artificial freshwater with different combinations of Na^+ and Cl^- indicated that the function of Cl^- uptake, but not Na^+ uptake, is associated with the morphology of gill MR cells (8, 9). Taking all this into account, it is possible that these HR cells and NaR cells are responsible for different ion transports. H^+ secretion in HR cells implies that Na^+ uptake may also occur in this cell for exchange, while Cl^- and/or Ca^{2+} uptake may be conducted in NaR cells. Recently, an epithelial type Ca^{2+} channel (ECaC), which is known to be required for transepithelial Ca^{2+} transport, has been cloned in zebrafish, and in situ hybridization with an antisense RNA probe demonstrated the expression of ECaC mRNA in NaR cells (28). Further studies using Cl^-- and Ca^{2+}-selective electrodes are needed to investigate whether Na^+, Cl^-, and Ca^{2+} uptake occur in different groups of ionocytes. HR cells and NaR cells may represent two subtypes of MR cells, or more precisely, ionocytes, because HR cells did not contain as many mitochondria as NaR cells.

The Na^+ pump has been found to be highly expressed in the tubular system (infolded basolateral membrane) of MR cells in seawater- and freshwater-adapted fish in a salinity-dependent manner. In this study, the immunofluorescence of the Na^+ pump in MR cells was usually distributed throughout the entire cell, with the exception of the nuclear region, and slightly outlined the basolateral tubular system. On the basis of immunolabeling of the Na^+ pump, several species of fish have been reported to develop MR cells in the skin of the larval stage, and these MR cells are suggested to function in ion transport (17, 20). Canfield and coworkers (6) hybridized Na^+ pump α-subunit transcripts in the skin of developing zebrafish and referred to those Na^+-pump-expressing cells as mucus cells. Hsiao and coworkers (16) also reported parvalbumin genes expressing in these mucus cells in zebrafish embryo. These reports were ignorant of the existence of ionocytes such as HR cells and NaR cells, which appear in the skin of zebrafish embryo as early as 24 h after fertilization in our observations. To date, there is no convincing evidence to support high expression of an Na^+ pump in mucus cells. The ultrastructure of skin mucus

cells is quite different from that of HR cells or NaR cells under transmission electron microscopy in our experience; moreover, there is no immunoreaction of the Na$^+$ pump or the H$^+$ pump found in these mucus cells (data not shown).

REFERENCES

1. **Ackermann GE and Paw BH.** Zebrafish: a genetic model for vertebrate organogenesis and human disorders. *Front Biosci* 8: d1227–d1253, 2003.
2. **Al-Awqati Q.** Plasticity in epithelial polarity of renal intercalated cells: targeting of the H$^+$-ATPase and band 3. *Am J Physiol Cell Physiol* 270: C1571–C1580, 1996.
3. **Briggs JP.** The zebrafish: a new model organism for integrative physiology. *Am J Physiol Regul Integr Comp Physiol* 282: R3–R9, 2002.
4. **Brown D and Breton S.** Mitochondria-rich, proton-secreting epithelial cells. *J Exp Biol* 199: 2345–2358, 1996.
5. **Brown D, Smith PJ, and Breton S.** Role of V-ATPase-rich cells in acidification of the male reproductive tract. *J Exp Biol* 200: 257–262, 1997.
6. **Canfield VA, Loppin B, Thisse B, Thisse C, Postlethwait JH, Mohideen MA, Rajarao SJ, and Levenson R.** Na,K-ATPase alpha and beta subunit genes exhibit unique expression patterns during zebrafish embryogenesis. *Mech Dev* 116: 51–59, 2002.
7. **Chang IC and Hwang PP.** Cl$^-$ uptake mechanism in freshwater-adapted tilapia (*Oreochromis mossambicus*). *Physiol Biochem Zool* 77: 406–414, 2004.
8. **Chang IC, Lee TH, Yang CH, Wei YY, Chou FI, and Hwang PP.** Morphology and function of gill mitochondria-rich cells in fish acclimated to different environments. *Physiol Biochem Zool* 74: 111–119, 2001.
9. **Chang IC, Wei YY, Chou FI, and Hwang PP.** Stimulation of Cl$^-$ uptake and morphological changes in gill mitochondria-rich cells in freshwater tilapia (*Oreochromis mossambicus*). *Physiol Biochem Zool* 76: 544–552, 2003.
10. **Claiborne JB, Edwards SL, and Morrison-Shetlar AI.** Acid-base regulation in fishes: cellular and molecular mechanisms. *J Exp Zool* 293: 302–319, 2002.
11. **Ehrenfeld J and Klein U.** The key role of the H$^+$ V-ATPase in acid-base balance and Na$^+$ transport processes in frog skin. *J Exp Biol* 200: 247–256, 1997.
12. **Faszewski EE and Kunkel JG.** Covariance of ion flux measurements allows new interpretation of *Xenopus laevis* oocyte physiology. *J Exp Zool* 290: 652–661, 2001.
13. **Foskett JK and Scheffey C.** The chloride cell: definitive identification as the salt-secretory cell in teleosts. *Science* 215: 164–166, 1982.
14. **Goss GG, Adamia S, and Galvez F.** Peanut lectin binds to a subpopulation of mitochondria-rich cells in the rainbow trout gill epithelium. *Am J Physiol Regul Integr Comp Physiol* 281: R1718–R1725, 2001.
15. **Hiroi J, Kaneko T, and Tanaka M.** In vivo sequential changes in chloride cell morphology in the yolk-sac membrane of Mozambique tilapia (*Oreochromis mossambicus*) embryos and larvae during seawater adaptation. *J Exp Biol* 202: 3485–3495, 1999.
16. **Hsiao CD, Tsai WY, and Tsai HJ.** Isolation and expression of two zebrafish homologues of parvalbumin genes related to chicken CPV3 and mammalian oncomodulin. *Mech Dev* 119: S161–166, 2002.
17. **Hwang PP, Lee TH, Weng CF, Fang MJ, and Cho GY.** Presence of Na-K-ATPase in mitochondria-rich cells in the yolk-sac epithelium of larvae of the teleost *Oreochromis mossambicus*. *Physiol Biochem Zool* 72: 138–144, 1999.
18. **Jaffe LF and Levy S.** Calcium gradients measured with a vibrating calcium-selective electrode. *Inst Elect Eng Med Biol Soc Conf* 9: 779–781, 1987.
19. **Jaffe LF and Nuccitelli R.** An ultrasensitive vibrating probe for measuring steady extracellular currents. *J Cell Biol* 63: 614–628, 1974.
20. **Kaneko T, Shiraishi K, Katoh F, Hasegawa S, and Hiroi J.** Chloride cells during early life stages of fish and their functional differentiation. *Fisheries Sci* 68: 1–9, 2002.
21. **Katoh F, Hyodo S, and Kaneko T.** Vacuolar-type proton pump in the basolateral plasma membrane energizes ion uptake in branchial mitochondria-rich cells of killifish *Fundulus heteroclitus*, adapted to a low ion environment. *J Exp Biol* 206: 793–803, 2003.
22. **Kuhtreiber WM and Jaffe LF.** Detection of extracellular calcium gradients with a calcium-specific vibrating electrode. *J Cell Biol* 110: 1565–1573, 1990.
23. **Larsen EH, Christoffersen BC, Jensen LJ, Sorensen JB, and Willumsen NJ.** Role of mitochondria-rich cells in epithelial chloride uptake. *Exp Physiol* 81: 525–534, 1996.
24. **Lin LY and Hwang PP.** Mitochondria-rich cell activity in the yolk-sac membrane of tilapia (*Oreochromis mossambicus*) larvae acclimatized to different ambient chloride levels. *J Exp Biol* 77: 406–414, 2004.
25. **Lin LY and Hwang PP.** Modification of morphology and function of integument mitochondria-rich cells in tilapia larvae (*Oreochromis mossambicus*) acclimated to ambient chloride levels. *Physiol Biochem Zool* 74: 469–476, 2001.
26. **Lin H, Pfeiffer D, Vogl A, Pan J, and Randall D.** Immunolocaliztion of H$^+$-ATPase in the gill epithelia of rainbow trout. *J Exp Biol* 195: 169–183, 1994.
27. **Marshall WS.** Na$^+$, Cl$^-$, Ca^{2+} and Zn^{2+} transport by fish gills: retrospective review and prospective synthesis. *J Exp Zool* 293: 264–283, 2002.
28. **Pan TC, Liao BK, Huang CJ, Lin LY, and Hwang PP.** Epithelial Ca^{2+} channel expression and Ca^{2+} uptake in developing zebrafish. *Am J Physiol Regul Integr Comp Physiol* 289: R1202–R1211, 2005.
29. **Perry SF.** The chloride cell: structure and function in the gills of freshwater fishes. *Annu Rev Physiol* 59: 325–347, 1997.
30. **Pisam M, Massa F, Jammet C, and Prunet P.** Chronology of the appearance of β, A, and α mitochondria-rich cells in the gill epithelium during ontogenesis of the brown trout (*Salmo trutta*). *Anat Rec* 259: 301–311, 2000.
31. **Reid SD, Hawkings GS, Galvez F, and Goss GG.** Localization and characterization of phenamil-sensitive Na$^+$ influx in isolated rainbow trout gill epithelial cells. *J Exp Biol* 206: 551–559, 2003.
32. **Smith PJ, Hammar K, Porterfield DM, Sanger RH, and Trimarchi JR.** Self-referencing, non-invasive, ion selective electrode for single cell detection of trans-plasma membrane calcium flux. *Microsc Res Tech* 46: 398–417, 1999.
33. **Smith PJ and Trimarchi J.** Noninvasive measurement of hydrogen and potassium ion flux from single cells and epithelial structures. *Am J Physiol Cell Physiol* 280: C1–C11, 2001.
34. **Van Der Heijden AJH, Verbost PM, Eygensteyn J, Li J, Wendelaar Bonga SE, and Flik G.** Mitochondria-rich cells in gills of tilapia (*Oreochromis mossambicus*) adapted to fresh water or seawater: quantification by confocal laser scanning microscopy. *J Exp Biol* 200: 55–64, 1997.
35. **Wilson JM, Laurent P, Tufts BL, Benos DJ, Donowitz M, Vogl AW, and Randall DJ.** NaCl uptake by the branchial epithelium in freshwater teleost fish: an immunological approach to ion-transport protein localization. *J Exp Biol* 203: 2279–2296, 2000.